



AQUADA: Automated quantification of damages in composite wind turbine blades for LCOE reduction

Chen, Xiao; Shihavuddin, ASM; Madsen, Steen Hjelm; Thomsen, Kenneth; Rasmussen, Steffen; Branner, Kim

Published in:
Wind Energy

Link to article, DOI:
[10.1002/we.2587](https://doi.org/10.1002/we.2587)

Publication date:
2021

Document Version
Publisher's PDF, also known as Version of record

[Link back to DTU Orbit](#)

Citation (APA):
Chen, X., Shihavuddin, ASM., Madsen, S. H., Thomsen, K., Rasmussen, S., & Branner, K. (2021). AQUADA: Automated quantification of damages in composite wind turbine blades for LCOE reduction. *Wind Energy*, 24(6), 535-548. <https://doi.org/10.1002/we.2587>

General rights

Copyright and moral rights for the publications made accessible in the public portal are retained by the authors and/or other copyright owners and it is a condition of accessing publications that users recognise and abide by the legal requirements associated with these rights.




- Users may download and print one copy of any publication from the public portal for the purpose of private study or research.
- You may not further distribute the material or use it for any profit-making activity or commercial gain
- You may freely distribute the URL identifying the publication in the public portal

If you believe that this document breaches copyright please contact us providing details, and we will remove access to the work immediately and investigate your claim.

RESEARCH ARTICLE

WILEY

AQUADA: Automated quantification of damages in composite wind turbine blades for LCOE reduction

Xiao Chen¹  | ASM Shihavuddin²  | Steen Hjelm Madsen¹ |
Kenneth Thomsen¹ | Steffen Rasmussen¹ | Kim Branner¹ 

¹Department of Wind Energy, Technical University of Denmark, Roskilde, Denmark

²EEE Department, Green University of Bangladesh, Dhaka, Bangladesh

Correspondence

Xiao Chen, Department of Wind Energy, Technical University of Denmark, Frederiksborgvej 399, 4000 Roskilde, Denmark.
Email: xiac@dtu.dk

Funding information

Danish Energy Technology Development and Demonstration Program, Grant/Award Number: 64016-0023; Innovationsfonden, Grant/Award Number: 6151-00020B; DARWIN Project

Abstract

Reliability and cost are two important driving factors in the development of wind energy. Automation and digitalization of operation and maintenance (O&M) procedures help to increase turbine reliability and reduce the levelized cost of energy (LCOE). Here, we demonstrate a novel method, coined as AQUADA, which may change the current labor-intensive and operation-interfering blade inspection by using thermography and computer vision. We experimentally show that structural damages below the surfaces can be detected and quantified remotely when wind turbine blades are subject to fatigue loads. The data acquisition and analysis are automatically done in one single step, which may shift the current inspection paradigm through more automated O&M procedures. The cost analysis shows that the AQUADA method has a potential to at least half the total inspection cost and reduce the LCOE by 1%–2% when applied to a baseline land-based wind farm consisting of twenty 2.45-MW turbines. All data and source codes are published for researchers to reproduce our results and facilitate further development of AQUADA towards more mature industrial applications.

KEYWORDS

composite blades, computer vision, damage inspection, digitalization, fatigue, operation and maintenance, thermography

1 | INTRODUCTION

Smart solutions such as automation and digitalization can contribute to levelized cost of energy (LCOE) reduction of wind energy, which remains the overall driver for the development of the wind energy.^{1–6} Typically, the operation and maintenance (O&M) costs account for 20%–25% of the total LCOE for both onshore and offshore wind.⁷ An important way to reduce the O&M cost is to identify and quantify the hidden damages and at the same time make the inspection cheaper and less labor-intensive by automation and digitalization.⁸

Current wind turbine blade inspection primarily uses rope and/or basket access techniques, ground-based cameras, and flying drones.^{9–14} These methods are dominantly based on optical images at frequencies visual to the human eyes. Only the images of damages and features on the surface such as erosion, dirt, and surface cracks are acquired.¹⁵ Indeed, the critical damages often occur underneath the blade surface,^{16,17} and they are hidden from the view especially from afar. This is, at least partly, the reason why the more labor-intensive and expensive rope and/or basket access method is still widely used in the industry.⁹ After the image acquisition, a significant amount of expert man-hours is still needed to analyze

This is an open access article under the terms of the Creative Commons Attribution License, which permits use, distribution and reproduction in any medium, provided the original work is properly cited.

© 2020 The Authors. Wind Energy published by John Wiley & Sons Ltd.

the inspection images and categorize blade damages qualitatively.^{9–14} This process requires considerable manual effort and is prone to human error. On top of that, wind turbine operation has to be stopped during the inspection, incurring additional cost due to downtime and lost revenue.

In this study, we demonstrate a novel method, coined as AQUADA, which may potentially overcome some of the aforementioned limitations of existing inspection methods. We automatically quantify damages remotely using thermography and computer vision techniques. First, we test a full-scale wind turbine blade under fatigue loads in the laboratory using a biaxial fatigue exciter. Thermal images of the blade are taken from afar and thermal footprints generated by blade damages are identified. Next, we develop a thermal image analysis tool to automatize the pipeline of damage identification, localization, segmentation, and quantification in one single step. Then, we validate the developed tool using material tests. Finally, we perform a cost analysis to assess the potential impact of the AQUADA method on the LCOE reduction using an onshore wind farm as a baseline.

We find the developed AQUADA cannot only identify structural damages but also quantify them in real-time as the thermal images are taken. Comparing to optical RGB image-based inspection, the AQUADA method can detect subsurface damages while neglecting prevalent surface features that are irrelevant to the structural integrity. The AQUADA method is automated and potentially does not require interruption of the normal operation of wind turbines. We find the total inspection cost can be at least halved and the LCOE reduction is estimated to be 1%–2% when applied to a baseline onshore wind farm consisting of 20 2.45-MW turbines. This laboratory demonstration shows a possibility that the AQUADA method may change the current labor-intensive and operation-interfering inspection paradigm in the wind energy industry.

2 | EXPERIMENT

We demonstrate the AQUADA method in the laboratory. A 14.3-m full-scale wind turbine blade is tested under biaxial fatigue that mimics more realistic combined loading conditions in operation. The test is conducted in the DTU Large Scale Test Facility, in which the temperature is constant. The blade is mounted on a test stand and is loaded by a ground-based exciter to simulate the operational load conditions of the blade in the field, see Figure 1. An infrared thermal camera is placed 9.3 m above the ground and measures the temperature of the blade during the test. A regular optical camera is placed at the same location to provide ground truth images for comparison. The distance between the thermal camera and the blade is comparable to the distances when a drone with a thermal camera is used in the field inspection with the turbine halted.¹⁸ Although no drone is used in this study, the test setups are made to mimic the inspection distance when the thermal camera is mounted on a drone.

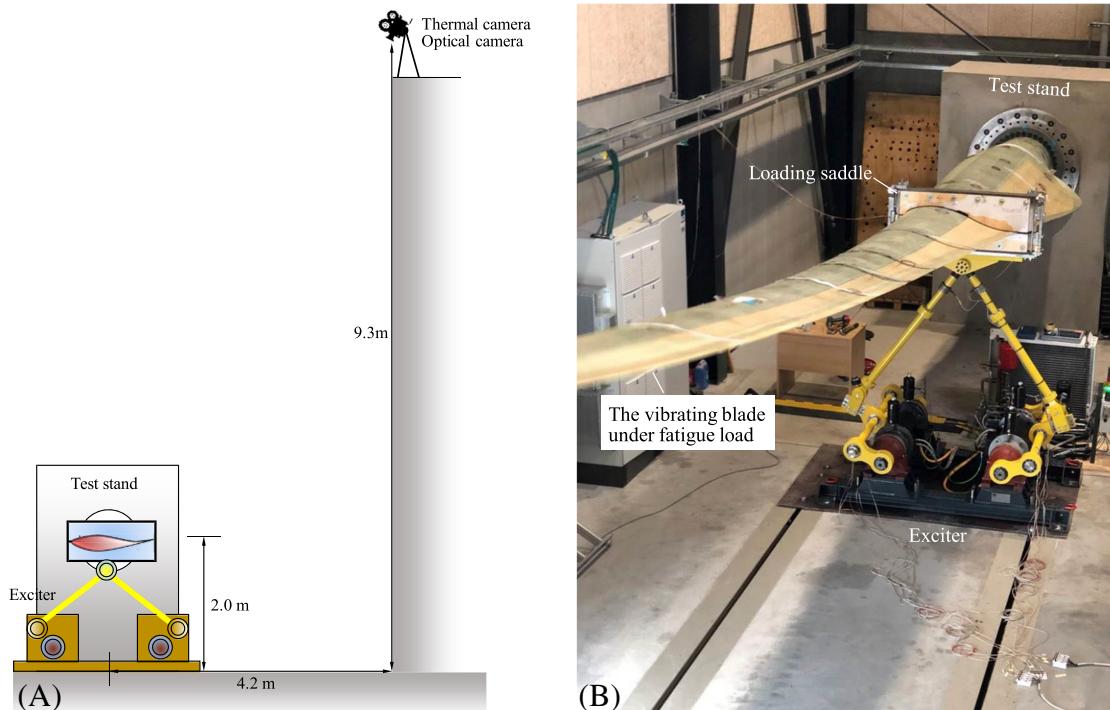


FIGURE 1 The test setup of the blade under a fatigue test. (A) The overall test setup viewed from the blade tip towards the blade root. The blade is mounted on a test stand with its suction side facing the ground. A thermal camera and an optical camera take images from 9.3 m above the ground. (B) The blade under biaxial fatigue that is excited by a ground-based dual-axis exciter. The exciter applies both flapwise and edgewise loading simultaneously to the blade, mimicking combined loading conditions of the blade in operation

2.1 | The blade

A 14.3-m commercial blade is used in the study. The blade is made of fiberglass/polyester composite materials and has two shear webs bonded to spar caps. The majority part of the blade is unpainted. Unidirectional, biaxial, and triaxial laminates, chopped fiber mats, and PVC foams were used to manufacture the blade. The material properties information is provided in Table 1. The blade has been tested under standard static and fatigue loading following IEC 64100-23 used for blade certification.¹⁹ After these tests, neither damages nor stiffness degradation has been found in the blade. Six artificial damages are introduced into the blade to trigger damage progress under fatigue loading, Figure 2. These artificial damages were made by cutting the blade using a grinder with a diamond disc with a thickness of 2 mm. The focus of the test is to examine the thermal footprints of progressive damages, so it is considered to be less important how the damages were introduced. In addition to the progressive damages triggered by artificial damages, those initiated from manufacturing-induced defects and structural geometry transition are also investigated.

2.2 | Fatigue test

A dual-axis exciter is used to test the blade under biaxial fatigue. The test setup is to mimic realistic combined loading conditions that would be experienced by the blade in operation. The exciter is an electro actuated ground-based exciter. It applies controlled dynamic forces to the blade driving it into oscillating motion. Forces can be applied in a flapwise or edgewise direction or their combination. The actuation is procured by hollow shaft permanent magnet synchronous machines. Two gears are mounted on each machine in a pretensioned mechanical loop constraining backlash in the gearboxes. Torque arms are mounted on the output shaft side of the gears and deliver forces to pushrods via rod end link bearings. Pushrod top end link bearings are attached to a common axle and direct forces into a yoke attached to the blade. The exciter applies a cyclic force with a fatigue load amplitude of ± 8400 N at 2.25 Hz and ± 1200 N at 4.37 Hz in flapwise and edgewise direction, respectively. The fatigue test leads to cyclic strains which range from 1000 to 4000 microstrain in the spar caps of the blade along the blade spanwise location. The detailed fatigue test set up will be published in a separate study as it is less relevant to the main objective of the current work.

2.3 | Thermal imaging

The IR thermal camera FLIR A655SC is used in this study. The camera has an uncooled microbolometer detector with a resolution of 640×480 pixels and a pitch of $17 \mu\text{m}$. The accuracy of measurement is $\pm 2^\circ\text{C}$ or $\pm 2\%$ of reading. The thermal sensitivity measured by noise equivalent temperature difference (NETD) is <30 mK. The field of view (FoV) is $25^\circ \times 19^\circ$. The weight of the camera is 0.90 kg, and the size is

TABLE 1 Material properties of fiberglass/polyester composites and PVC foam used in the blade^a

Material	E_{11}	E_{22}	E_{33}	G_{12}	G_{13}	G_{23}	u_{12}	u_{13}	u_{23}
Uniax laminate	1.00	0.35	0.35	0.12	0.12	0.12	0.24	0.09	0.48
Biax laminate	1.00	1.00	1.00	0.83	0.83	0.49	0.53	0.19	0.02
Triax laminate	1.00	0.66	0.66	0.42	0.42	0.31	0.48	0.01	0.08
Chop fiber mat	1.00	1.00	0.54	0.35	0.16	0.16	0.32	0.20	0.35
PVC foam	1.00	1.00	1.00	0.36	0.36	0.36	0.40	0.40	0.40

^aAll moduli are normalized by E_{11} . Poisson's ratios are the original values without normalization. Subscripts 1, 2, and 3 mean longitudinal, transverse, and through-thickness direction, respectively.

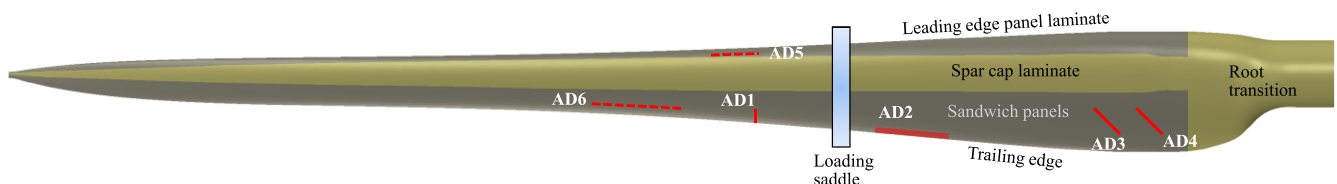


FIGURE 2 The artificial damages (AD) introduced in the blade. They are produced by cutting laminates, sandwich panels, and adhesive bondlines using a diamond saw. The focus of the test is to examine the thermal footprints of progressive damages, so it is considered to be less important how the damages were introduced. Only the artificial damages on the pressure side facing the cameras are investigated by thermal imaging in this study and they are depicted with solid lines. The blade is encastered on a test stand and fatigue loaded at 5.3 m where a loading saddle is connected to the ground-based exciter

216 × 73 × 75 mm. When taking thermal videos, no zooming is applied, and only the focus of the thermal camera is adjusted. Most thermal videos are taken when the thermal camera is placed 9.3 m above the ground. A few close-up images are also taken to identify the local thermal features and their causes. Besides, the optical images are taken by the regular optical camera when visual inspections are carried out. They provide the ground truth data for the verification against the thermal images of the fatigue damages during the test.

2.4 | Test results

During the fatigue test, blade damages initiate from artificially introduced damages, sharp geometric transitions, and manufacturing-induced defects. When the blade damages progress, they generate thermal footprints due to rubbing and friction of materials along and inside cracks,^{20,21} which distinguish them from the surface features that are captured in optical images but irrelevant to the structural integrity. Figure 3 shows a comparison between a thermal and an optical image of a blade region where the artificial damage, that is, a transverse cut through the entire trailing edge, has been introduced. During the test, a hot spot appears in the thermal image due to a significant local heat up at the crack growing from the tip of the transverse cut. The hot spot has a higher temperature than the rest of the blade, making it easy to be recognized. The blade

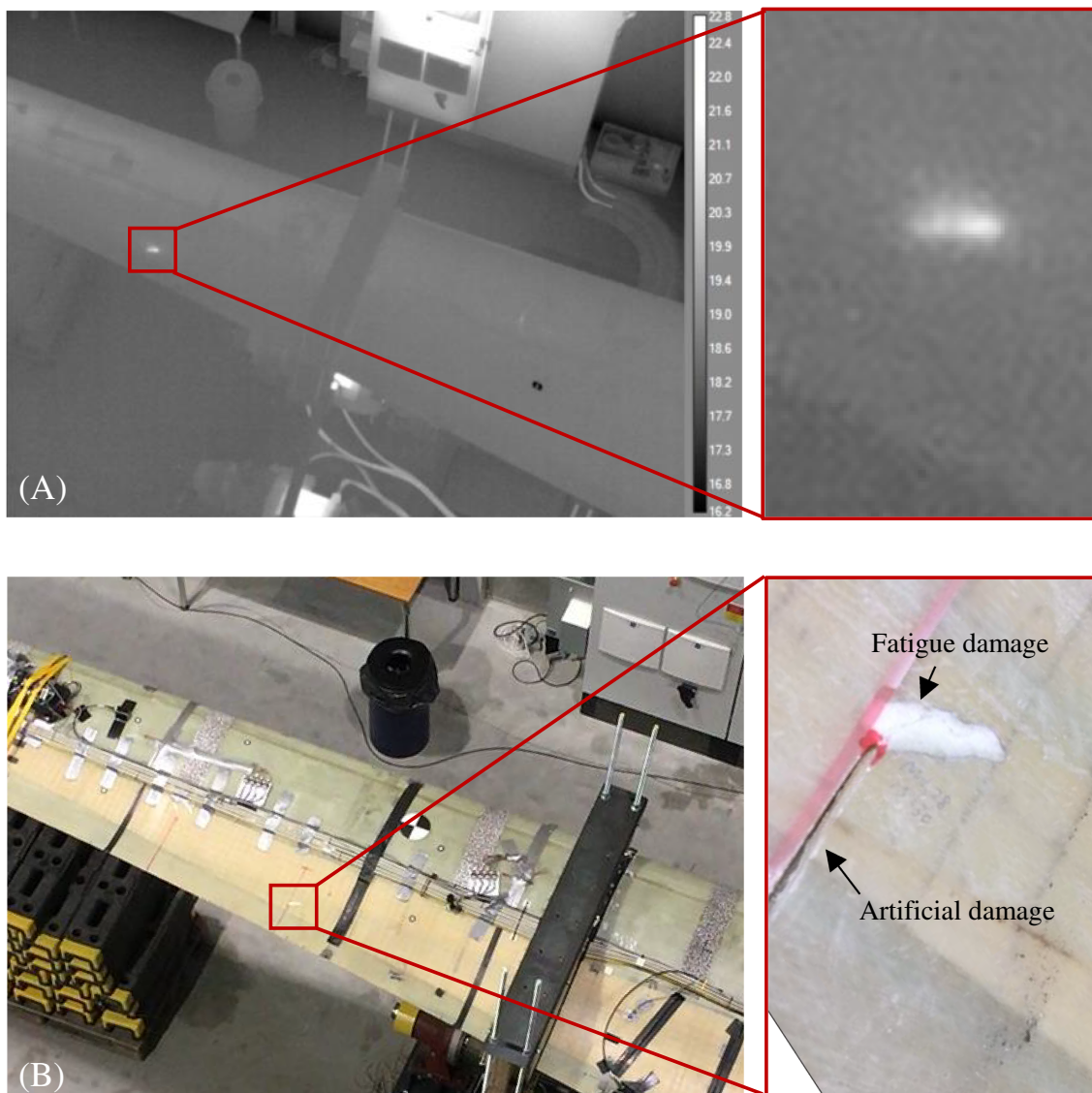


FIGURE 3 Fatigue damage initiates at the artificial damage during the blade test. (A) A thermal image of a local heat up at the tip of the artificial damage. Thermal footprints from the laboratory environment including the exciters are also captured in the image. (B) An optical image of the same location provides comparisons to the thermal image of the blade damage. Surface features, such as cables, markers, and tapes, that are prevalent in the optical image have negligible thermal footprints, making the blade damage under fatigue easy to identify

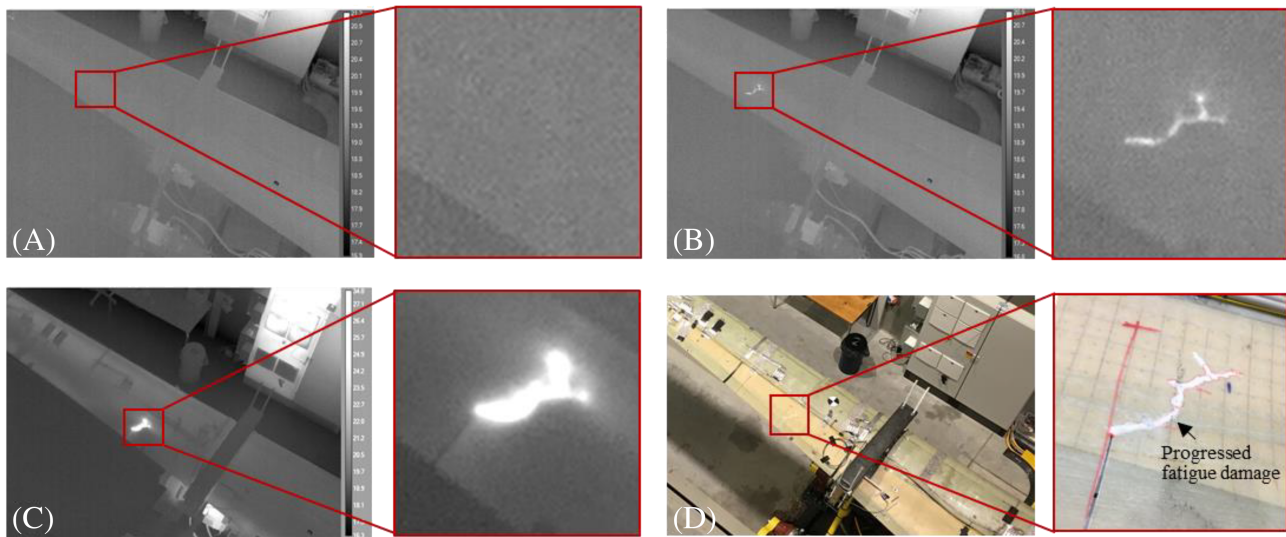


FIGURE 4 The thermal and optical images of the blade with progressed damages. (A) No thermal footprints is observed when no fatigue load is applied to the blade. (B) Soon after the fatigue test, the thermal contour shows the progressed damage compared to the previous observation when the blade is less fatigued. (C) The damage continues to progress and dissipate heat to the adjacent materials, prompting the increase of the damage size. (D) An optical image of the progressed damage showing that the complex geometry of the progressed damage is well captured by the thermal image

contains many surface features, such as cables, markers, and tapes, that are prevalent in the optical image but have negligible thermal footprints in the thermal image. It is difficult to identify the blade damage from the optical image without knowing its whereabouts a prior, but it is rather easy to locate the abnormalities from the thermal image. The actual geometry of the cracks agrees with that detected in the thermal image.

The blade damage progresses during the test. Figure 4 shows the thermal images of the blade in the same region with considerably progressed damage. When no fatigue loading is applied to the blade, no temperature variation is observed around the damaged region, Figure 4A. A short time after the fatigue loading, a clear thermal footprint appears with a larger size than the one detected when the blade is less fatigued, Figure 4B. Continuing fatigue loading causes the area of the thermal contour to increase due to more heat generated at the crack front where the crack is growing, prompting further damage progress. Figure 4C. An optical image of the damage, Figure 4D, shows that the thermal image captures the actual geometry of the progressed fatigue damage quite well.

Other regions of the blade show similar results. Figure 5 shows the thermal images of the blade region close to the root with comparison to their counterpart optical images. Remarkably, four hot spots are observed at two cracks introduced as artificial damages in the sandwich panels, Figure 5A,B. Besides, two distinct thermal footprints are found in the root transition region of the blade, Figure 5C. These two thermal footprints are generated naturally during the fatigue test as no artificial damages have been introduced there. An optical image, Figure 5D, shows that one thermal footprint is due to the subsurface damage in the form of delamination while the other is covered by filler and is visually unrecognizable. Inspection after removing the filler finds out that here exists subsurface damage in the form of laminate fracture in a vertical direction, agreeing with the detected thermal footprint in this location, see Figure 6.

The experimental results highlight the value of thermal imaging in detecting damages remotely when the blades are subject to operational loads. Instead of using an external heating source to excite thermal abnormalities,^{22–27} we do not apply any thermal excitation to the blade in this study. The thermal footprints of damages are generated when the blade is under fatigue. This has practical importance for the field application—there is no need to stop the normal operation of wind turbines during the inspection as required by the existing inspection methods used in the wind energy industry.^{9–14} Besides, both surface damages and subsurface damages can be detected, making inspection results structurally more meaningful compared to the visual inspections which only detect damages on the blade surface.

3 | IMAGE ANALYSIS

Several hundreds of images are often collected from one wind turbine inspection, and with wind farms typically having dozens, or even hundreds, of turbines, thousands of inspection images need to be processed and analyzed after each wind farm inspection.²⁸ According to the current industrial practice, image acquisition and image analysis are two sequential procedures, with the latter consuming a considerable amount of expert

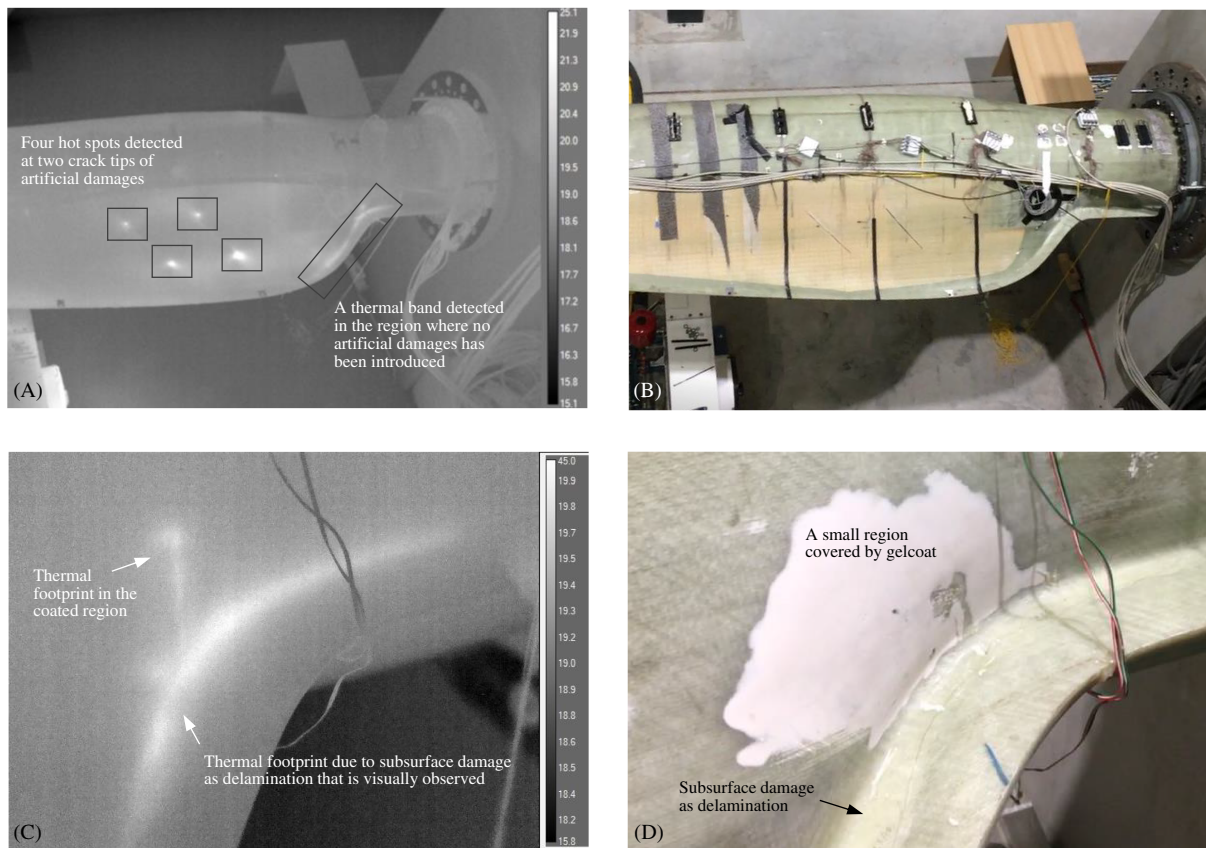


FIGURE 5 Blade damage detection in the blade root region during the fatigue test. (A) An overview of thermal footprints detected from multiple sites. (B) An optical image of the same region shows that the blade damages are unrecognizable amid many surface features. (C) A close-up of the thermal footprints shows two distinct thermal features, with one being the curved thermal band due to the visually apparent delamination and the other being a vertical band that is not visual due to the filler cover. (D) An optical image shows the visually apparent subsurface damage in the form of delamination and a small region covered by the filler. Actually, after a careful examination using a microscope, we found tiny surface cracks blinking in the coated region during the fatigue test. A significant vertical crack is found after the filler is removed and verifies the observed thermal footprint, see Figure 6

man-hours. In this study, we use a computer vision-based thermal image analysis pipeline to automatize data interpretation including damage identification and quantification in real-time as the images are taken.

3.1 | Blade damage quantification

Manual vision analysis of thermal images for blade damages is challenging in nature as there can be other objects with higher temperature response in the images taken from field.²⁹ The thermal image in Figure 7A exemplifies this situation and shows significant thermal footprints from the exciter and the laboratory environment besides that from the blade damage of interest. First, we use Hough transforms^{30,31} algorithm to detect lines in images to identify two edge lines of the blade, Figure 7B. This technique identifies the location of the blade with more than 99% accuracy, for example, correctly in 744 frames out of 750 frames in this example. Next, within the region of the identified blade location, a high-temperature location is searched using intensity thresholding.³² The location of the hot spot indicates the detected blade damage, Figure 7C. Once the location of the damage is identified, the area around it is cropped to further investigate the area with more details. The blade damages in consecutive frames are segmented based on intensity thresholding³² Figure 7D and later are skeletonized³³ to capture its detailed geometry, Figure 7E. The final result of the automated image process tool agrees with the optical image as shown in Figure 7F.

Considering that the damage progresses under fatigue and so does the size of its thermal footprint, we measure the size of the damage in the number of pixels within the damage segmentation in each thermal image video frame. After the blade is tested under fatigue for approximately 1.5 million cycles, we apply the automated image process tool to the thermal image video and count the number of pixels in the damage segmentation, see Figure 8. The data points show the size of the damage in the number of pixels changes with the number of fatigue cycles when the thermal image video is taken. A regression curve with a polynomial of fifth order is plotted in red color and it characterizes the damage growth

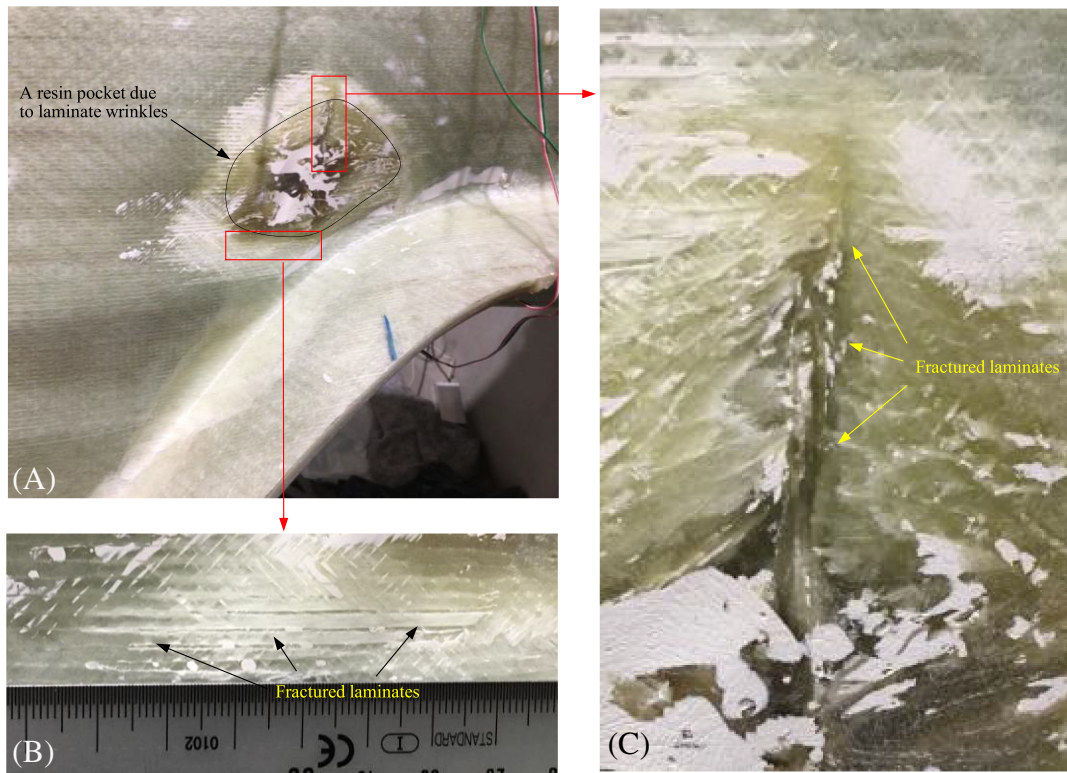


FIGURE 6 The close-up optical images of the region initially covered by the filler. The filler is removed to verify detection from the thermal images of Figure 5C. (A) The exposed region is found to have had a resin pocket due to internal damage in the form of laminate wrinkles induced during manufacturing. (B) The subsurface damage in the form of laminate fracture is observed as longitudinal cracks, which show noticeable, although not significant, thermal footprints in Figure 5C in the main manuscript. (C) The subsurface damage in the form of laminate fracture due to wrinkles runs vertically, leading to a significant thermal footprint that can be detected even when it was covered by the filler as shown in Figure 5C,D

over time. This result provides essential information on the quantitative damage state such as the growth rate. Video S1 illustrates the temporal formation for the damage automatically detected, tracked, and quantified using the AQUADA method. With this automated thermal image process tool, image acquisition and image analysis, instead of being two sequential procedures, now can be integrated into one single step, enabling fast, reliable, and quantitative inspection. The original thermal video and the source codes of the developed tool are provided in Video S2 and Supporting Information codes, respectively.

In this work, we deployed a thresholding based approach for detecting the image. The threshold that differentiates the damages is chosen by studying the distribution of thermal energy across the entire blade and the damage locations. The same threshold value has been used across all experiments as the experimental setup stays consistent, see Supporting Information codes where the source codes of the image process tool are provided. The drone-based inspection in the field may require a more sophisticated detection method based on a deep learning framework, which would be part of our future extension of the system.

3.2 | Validation test

To prove that the damage state quantified by the thermal image process tool truly reflects the actual physical damage, we conduct material tests and compare the mechanically measured damage state to that obtained from the image process tool. Six precracked sandwich specimens similar to these used in the blade are tested under uniaxial fatigue, see Figure 9. Six sandwich specimens are made by vacuum infusion using biaxial glass fiber fabrics, PVC foams, and epoxy, that is, $[\pm 45_2/\text{Foam}/\pm 45_2]$. The nominal size of the specimens is 100 mm \times 400 mm \times 13 mm. They are precracked and three sandwich specimens are painted whereas the other three are unpainted. Tension-tension fatigue is applied to all specimens with $R = 0.1$. The stiffness of the specimens at the i th cycle is the slope, E_i , from the linear regression of the measured stress-strain curve. The stiffness loss is defined as $1 - E_i/E_0$, where E_0 is the initial stiffness. The damping of the specimens, D_i , is defined by the normalized energy loss in the material during the i th cycle, and it is measured by the area of the stress-strain hysteresis divided by the reference area based on the

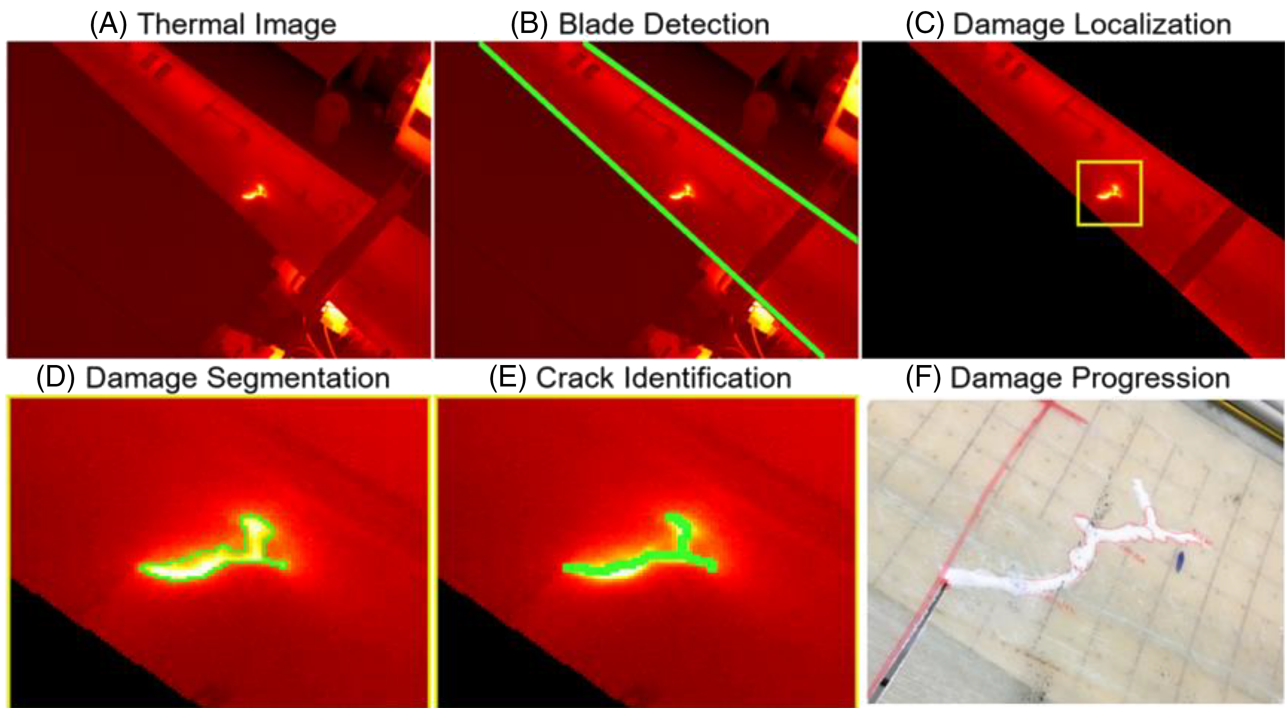


FIGURE 7 The automated analysis tool works on the thermal image. (A) the original thermal image taken from the thermal camera includes thermal footprints of the blade damage of interest, the exciter and the laboratory environment. (B) Detection of blade edges enables the identification of the blade within which the thermal footprints are of interest. (C) The damage is localized within the blade with other thermal abnormalities outside of the blade neglected. (D) Segmenting the damage based on intensity thresholding. (E) Identifying the crack by skeletonizing the damage segmentation to detail the damage geometry. (F) An optical image of the damage showing the detailed crack geometry agrees with the final result of the automated image process tool. All the thermal images are presented in a Redhot color map for better visualization and green colors are presented as positive detections

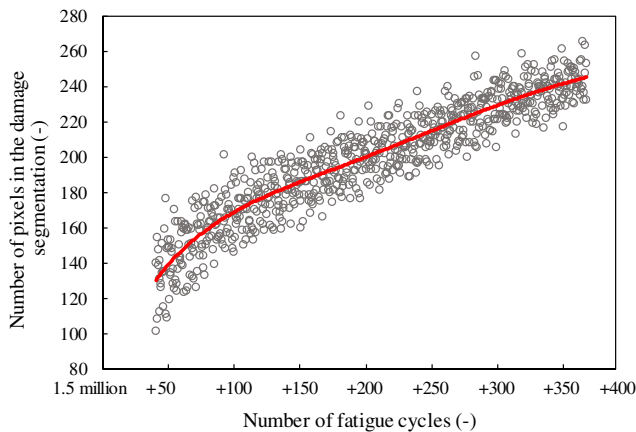


FIGURE 8 Scatter plot of the number of pixels in the damage segmentation with the increase of the fatigue cycle number. A fifth-order polynomial fitting shown in a red curve shows the gradual growth of the damage size. Noting the slope of the curve remains the same after the initial fatigue cycles. See Video S1

amplitudes of the strain and the stress of the i th cycle. A thermal camera takes thermal images regularly throughout the fatigue test until the specimens fail. An RGB optical camera is synchronized to take optical images for the ground-truth comparison. The thermal image process tool quantifies the damage state which agrees with the stiffness loss and the damping measured during the fatigue.

The damage state of the specimens is measured as the degradation of mechanical properties, that is, the stiffness loss and the increase of damping with the number of fatigue cycles. Thermal images of the specimens under fatigue are taken and processed using the developed tool to count the number of pixels in the damage segmentation. Figure 10 shows the results from one exemplary specimen. It can be seen that the damage state quantified by the tool agrees well with two mechanical measurements during the entire fatigue life, proving that the developed tool can be used as a reliable quantitative remote measurement of the physical damage state.

FIGURE 9 Validation test. The precracked sandwich specimen under fatigue loading with an optical and thermal camera taking images in the entire test. The damage state of the specimen is mechanically measured with the increase of fatigue cycles. The measured damage state is compared with the one quantified using the developed image process tool. In total, six specimens are tested and all results showed a similar trend to the one presented in Figure 10. The detailed test validation campaign will be published in a separate work as it is outside of the scope of the current focus in this study

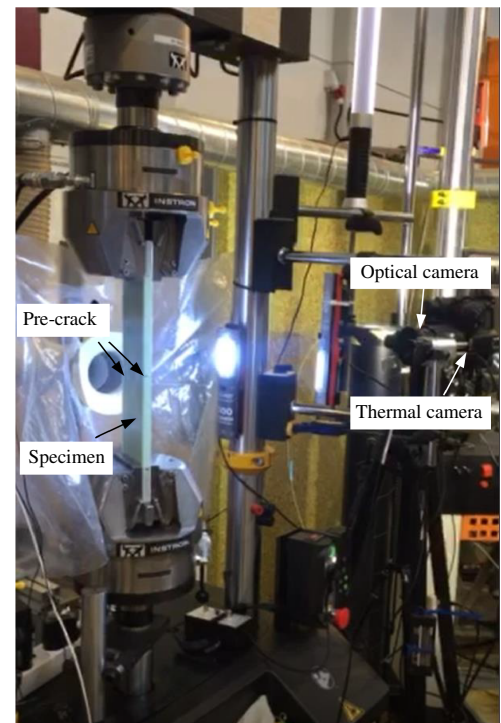
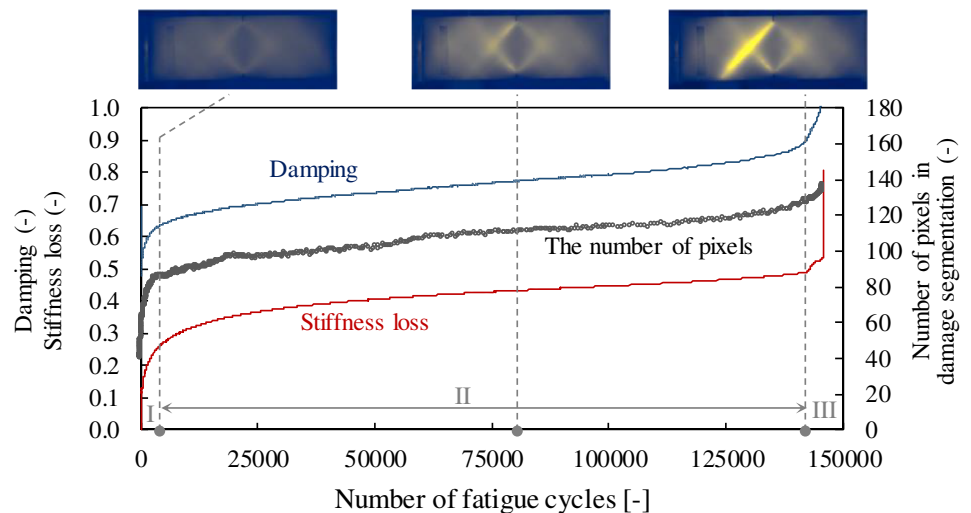


FIGURE 10 The damage state quantified by the image process tool agrees well with the stiffness loss and the damping of the specimen that are mechanically measured from the test. Three distinct phases, I: start, II: stable, III: fail, are observed during the fatigue life shown together with typical thermal images. A constant slope of the curve indicates a stable damage growth in phase II, in which an increase of slope characterizes a phase III response as the specimen approaches failure



4 | COST ANALYSIS

The AQUADA method may reduce inspection time and cost. To estimate the potential reduction of the total inspection cost of wind turbine blades, we analyze inspection speed, inspection cost, and data analysis cost of commonly used inspection methods. The data are obtained from several wind turbine O&M service companies based in China, Europe, and the United States for both 3- and 8-MW wind turbines, Table 2. Only the data for the 3-MW wind turbines are used for LCOE calculation. The new AQUADA method can be used on drones, sharing the same inspection time as the current drone-based inspection method but does not incur the cost of data analysis and turbine downtime, leading to at least the half of the total inspection cost used by the conventional methods.

Three conventional methods under investigation are manual inspection with rope or basket access, the ground-based inspection, and the drone-based inspection. The total inspection cost primarily consists of the cost of inspection itself, the data analysis cost and the cost of lost production during the inspection due to downtime. Among them, the inspection cost is associated with fieldwork and varies considerably depending on the inspection method; the data analysis cost is associated with analyzing and interpreting the acquired images, and is assumed to be the same

TABLE 2 Cost estimation of blade inspection using different methods

Inspection Method	Data Source	Inspection Speed	Inspection Cost	Data Analysis Cost	Lost Production 3 MW	Lost Production 8 MW	Total Cost 3 MW	Total Cost 8 MW
		h/blade	\$/turbine	\$/turbine	\$/turbine	\$/turbine	\$/turbine	\$/turbine
Manual (rope, basket)	<i>a</i>	1.5	800	400	675	1800	1875	3000
	<i>b</i>	2.0	2500*	400	900	2400	3800	5300
	<i>c</i>	0.8–2.0	1200–2500	400	360–900	960–2400	1960–3800	2560–5800
Ground based	<i>a</i>	1.0*	450	400	450	1200	1300	2050
	<i>b</i>	1.0	800	400	450	1200	1650	2400
	<i>c</i>	0.6–1.0	500*–800*	400	270–450	720–1,200	1170–1650	1620–2400
Drone based	<i>a</i>	0.33	300	400	148.5	396	848.5	1096
	<i>b</i>	0.3–0.4	300–500	400	135–180	360–480	835–1080	1060–1380
	<i>c</i>	0.3–0.6	270–540	400	135–270	360–720	805–1210	1030–1660
	<i>d</i>	0.3*–0.5*	400	400	135–225	360–600	935–1025	1160–1400
AQUADA	-	0.3–0.6	270–540	0	0	0	270–540	270–540

Note. Inspection speed, inspection cost, and data analysis cost are obtained from several wind turbine O&M service companies based in China, Europe, and the United States. The company names are shown as *a*, *b*, *c*, and *d* for the sake of anonymity. Despite the difference in inspection cost due to different labor costs, the inspection speed shows good consistency. The numbers with * are assumed numbers based on the available numbers from the same category. A 50% rated power is used to calculate lost production. \$0.1/kwh is used to calculate the cost of wind power. Despite the difference in blade size, the inspection speed is assumed to be the same for 3- and 8-MW wind turbines. The data analysis cost is assumed to be the same for all conventional inspection methods.

independent of the inspection method; the cost due to the turbine downtime depends on the inspection time, the power the wind turbine generates and the current electric power market price.

The data show that for a 3-MW wind turbine the total inspection costs are \$1875–\$3800 for the manual inspection, \$1170–\$1650 for the ground-based inspection, and \$805–\$1210 for the drone-based inspection. For an 8-MW wind turbine, the total inspection costs are 30%–60% higher for the manual inspection, 40%–60% higher for the ground-based inspection, and around 30% higher for the drone-based inspection. The proposed AQUADA method, once implemented in field application, is expected to use the same amount of inspection time as the drone-based method but with no or little additional cost incurred from data analysis and turbine downtime, leading to an estimated inspection cost of \$270–\$540 per turbine per inspection, which at least halves the total inspection cost of other methods.

The DTU Simplified Cost model, see Appendix A and Supporting Information, is used to quantify the impact of the AQUADA method on the LCOE. A baseline of a representative turbine is used to calculate the baseline LCOE using the conventional inspection method using an Excel tool. This baseline is defined based on average market numbers for US land-based turbines with a rated power of 2.45 MW and a rotor diameter of 116 m by the end of 2018.³⁴ This leads to an average specific power of 232 W/m². We use the inspection cost data of a 3-MW wind turbine in the LCOE calculation. We assume an average capacity factor is 35% and an annual declination factor on the production is 1.5%, which results in a loss of 26% in year 20 during a 20-year service period. Two inspections per year with each manual inspection cost per blade of \$3800. For the operational expenditures (OPEX), we assume \$27.9/kW/year. The total OPEX cost per turbine is thus \$68,355/year. With these key parameters, the LCOE of the baseline is calculated to be \$35.4/MWh.

For the new AQUADA method, two main differences are important for the LCOE calculation, and they are the change in OPEX and the change in annual energy production (AEP). The changes of these two numbers are derived from various inputs for actual cases provided by turbine manufacturers and developers. Considering the inspection cost of \$540 for the AQUADA method, the OPEX cost is calculated to be \$62,716/year per turbine, or \$25.6/kW/year when converted to the specific OPEX. This value can be directly compared to the baseline number of \$27.9/kW/year. With a negligible 0.1% increase in AEP due to the reduced downtime, the total LCOE reduction is calculated to be 2.6%. If both low-end inspection costs are used, that is, \$1875 for the baseline and \$270 for the new, the LCOE reduction is 1.3%. Calculations show that the AQUADA method reduces the LCOE by 0.8%–0.9% and 0.5%–0.6% when compared to the ground- and drone-based methods, respectively, see Table 3. Note that the economic loss incurred by blade failure, which might have been avoided using the AQUADA method due to its capability to detect hidden damages, is not taken into account in the LCOE calculation. Considering that the blade inspection usually uses a combination of three conventional inspection methods during the turbine's service life, an LCOE reduction of 1%–2% is expected if the AQUADA method is used.

Note that the cost model is based on a simplified cost scaling method for the turbine cost similar to the approach presented in Fingersh³⁵ and inspired by implementation from Stiesdal.³⁶ The baseline case is defined by the average numbers, characterizing turbines installed end 2018

TABLE 3 A summary of cost analysis using different inspection method on 2.45-WM land-based wind turbines

Inspection Method	Inspection Cost	The OPEX Cost Reduction	The Specific OPEX Reduction	The LCOE Reduction
	\$/turbine/inspection	\$/turbine/year	\$/kW/year	%
Manual	1875–3800	2776–5639	1.13–2.30	1.3–2.6
Ground-based	1170–1650	1557–1920	0.64–0.78	0.8–0.9
Drone-based	805–1210	925–1159	0.38–0.47	0.5–0.6
AQUADA	270–540	0	0	0

onshore in the US market.³⁴ We use a wind farm consisting of 20 2.45-MW turbines for the baseline, and the operational lifetime of the wind farm is 25 years. Considering two inspections per year, we obtain the baseline LCOE of 35.4 \$/MWh. Due to the AQUADA method, a reduction in OPEX and an increase in AEP are calculated based on the inspection cost data. The reduction in OPEX is considerable whereas the increase in AEP is negligible, leading to a total LCOE reduction ranging from 0.5% to 2.6% comparing to three conventional methods when the new AQUADA method is used.

5 | CONCLUDING REMARKS

Using thermography and computer-vision-based image processing, we experimentally demonstrate an automated, remote, and quantitative method, AQUADA, for smart wind turbine blade damage inspection. Comparing to the conventional inspection methods used in the industry, the main advantages of the proposed AQUADA method are fourfold: It detects structural damages below the blade surfaces; the image analysis is done at the same time as the images are acquired; it quantifies the physical damage state remotely and automatically; it potentially does not require the interruption of normal turbine operation; all those merits contribute to smart identification of blade damages, reducing the potential risk of expensive blade failure, and a significant reduction, at least by half, of the total inspection cost per turbine and an estimated LCOE reduction of 1%–2% compared to the baseline using conventional inspection methods.

AQUADA shows the possibility to have a cheaper and automatic inspection method of wind turbine blades. Inspections can be done more often and thereby reduce the risk of premature structural failure. The potential application could be autonomous drone inspection for offshore wind farms, which, comparing to the land-based wind farms, would yield more LCOE reduction. The AQUADA method is demonstrated in the laboratory, there are still some challenges for its field application. To name a few, first of all, not all damages can be detected and other NDT techniques and SHM methods still have to be used to obtain a complete picture of the damages in the blades; second, it might be a practical challenge to capture high-quality thermal images of a rotating blade, which has a tip speed of ranging from 80 to 100 m/s; third, the effects of undesired influences²⁹ such as sunlight reflections and varying environmental temperature on the detection results are not yet considered. Nevertheless, it is believed that the rapid advancement of the key enabling technologies (KET) such as drones and thermography will facilitate the further development of the AQUADA method. One other possible application may be a stationary thermal camera mounted on each turbine for structural health monitoring, just like, but much cheaper than, the current application of the light detection and ranging (LiDAR) technology in the wind energy industry.

It is beyond the scope of this study to demonstrate industrial applications. Nevertheless, the AQUADA method together with all shared data and source codes provides a possible pathway towards more frequent and reliable inspections without excessive costs which potentially brings a new paradigm of O&M to the industry and reduces the LCOE of the wind energy.

ACKNOWLEDGEMENTS

This study is partly funded by the DARWIN Project (Drone Application for pioneering Reporting in Wind turbine blade INSpections, 6151-00020B) from Innovation Fund Denmark. The blade fatigue exciter is developed by R&D A/S within the BLATIGUE project (Fast and Efficient Fatigue Test of Large Wind Turbine Blades, 64016-0023) funded by the Danish Energy Technology Development and Demonstration Program (EUDP), which also partly has funded the work. The author A.S. has not received any funding from the abovementioned projects. The blade was manufactured by Olsen Wings A/S. We would like to thank Janus Martin Thastum Jørgensen for describing the exciter. The authors are grateful to Prof. Anders BJORHOLM DAHL from DTU Compute for lending the IR thermal camera. The authors would also like to thank Peter BERRING for supporting in making the artificial damages, Süleyman Cem Yeniceli for evaluating cyclic strain ranges of the blade and Mattias Andersson for providing valuable comments to this study. We would like to thank the anonymous reviewers, who obviously are experts with extensive knowledge and experience in this area, for their constructive comments, valuable insights and helpful suggestions, which have helped us to improve the quality of this work from its original manuscript.

AUTHOR CONTRIBUTIONS

X.C. conceived the research. X.C. designed and carried out the blade test together with S.H.M. X.C. and S.H.M. collected and analyzed the inspection cost data. A.S. developed the image analysis tool with intense discussion with X.C. and wrote the image analysis section. K.T. conducted a cost analysis and wrote the LCOE section. S.R. conducted material tests together with X.C. and processed the test data. X.C. wrote the manuscript with contributions from other coauthors. K.B. provided valuable comments to this work and acquired funding to support this study.

CONFLICT OF INTERESTS

The authors declare no competing interests.

PEER REVIEW

The peer review history for this article is available at <https://publons.com/publon/10.1002/we.2587>.

ORCID

Xiao Chen  <https://orcid.org/0000-0001-6726-4068>

ASM Shihavuddin  <https://orcid.org/0000-0002-4137-9374>

Kim Branner  <https://orcid.org/0000-0002-9601-6343>

REFERENCES

1. Port of Rotterdam Part 1, 2, 3, 4, www.porttechnology.org, Accessed on May 3, 2020.
2. Veers P, Dykes K, Lantz E, et al. Grand challenges in the science of wind energy. *Science*. 2019;366(6464):1-9. <https://doi.org/10.1126/science.aau2027>
3. Lundquist JK, DuVivier KK, Kaffine D, Tomaszewski JM. Costs and consequences of wind turbine wake effects arising from uncoordinated wind energy development. *Nat Energy*. 2019;4(1):26-34.
4. Wisner R, Jenni K, Seel J, et al. Expert elicitation survey on future wind energy costs. *Nat Energy*. 2016;1(10):1-8.
5. Aabo C, Scharling Holm J, Jensen P, Andersson M, Lulu Neilsen E. MEGAVIND Wind Power Annual Research and Innovation Agenda; MEGAVIND: 2018.
6. Ziegler L, Gonzalez E, Rubert T, Smolka U, Melero JJ. Lifetime extension of onshore wind turbines: a review covering Germany, Spain, Denmark, and the UK. *Renew Sustain Energy Rev*. 2018;82:1261-1271.
7. Verbruggen, S. Onshore Wind Power Operations and Maintenance to 2018; New Energy Update: London, UK, 2016.
8. Stock-Williams C, Swamy SK. Automated daily maintenance planning for offshore wind farms. *Renew Energy*. 2018;133:1393-1403.
9. Bladena, Vattenfall, EON, Statkraft and KIRT x THOMSEN, Instruction Blade Inspections, retrieved on April 22, 2020.
10. Fedorov V. DARWIN—drone application for pioneering reporting in wind turbine blade Inspections, Wind Energy Denmark 2017, October 3, 2017, Herning, Denmark.
11. FORCE Technology, Drone inspection of wind turbines—on- and offshore, <https://forcetechnology.com/>, retrieved on Jan. 1st, 2020.
12. ABJ Drones, <https://abjdrones.com/>, retrieved on Jan. 1st, 2020.
13. Fauteux L, Jolin N. Drone solutions for wind turbine inspections, Nergica, December 2018.
14. Bley C. Drone blade inspections: Turning image collection into lifetime insight, Sandia wind turbine Blade workshop, August 29–September 1, 2016, Albuquerque, NM, USA.
15. Shihavuddin A, Chen X, Fedorov V, et al. Wind turbine surface damage detection by deep learning aided drone inspection analysis. *Energies*. 2019;12(676):1-12. <https://doi.org/10.3390/en12040676>
16. Chen X. Fracture of wind turbine blades in operation—part I: a comprehensive forensic investigation. *Wind Energy*. 2018;21(11):1046-1063. <https://doi.org/10.1002/we.2212>
17. Chen X. Experimental observation of fatigue degradation in a composite wind turbine blade. *Compos Struct*. 2019;212:547-551. <https://doi.org/10.1016/j.compstruct.2019.01.051>
18. Galleguillos C, Zorrilla A, Jimenez A, et al. Thermographic non-destructive inspection of wind turbine blades using unmanned aerial systems. *Plastics Rubber Compos*. 2015;44(3):98-103. <https://doi.org/10.1179/1743289815Y.0000000003>
19. International Electrotechnical Commission. *IEC Standard 61400-23, Wind Turbines—Part 23: Full-scale Structural Testing of Rotor Blades*. Edition 1 ed. 2014:2014-2004.
20. Beattie A, Rumsey M. Non-destructive evaluation of wind turbine blades using an infrared camera, 37th Aerospace Sciences Meeting and Exhibit. 11-14 January 1999, Reno, NV, U.S.A. <https://doi.org/10.2514/6.1999-46>
21. Rumsey M, Musial W. Application of infrared thermography nondestructive testing during wind turbine blade tests. *J Solar Energy Eng*. 2001;123(4):271-271.
22. Meinschmidt P, Aderhold J. Thermographic inspection of rotor blades, ECNDT 2006-Tu.1.5.3.
23. Lindberg J, Newman JW. Ground based inspection and monitoring of wind turbine blades, Sandia wind turbine blade workshop, August 29–September 1, 2016, Albuquerque, NM, USA.
24. Fey J, Djahan C, Mpouma TA, Neh-Awah J, Handmann U. Active thermographic structural feature inspection of wind-turbine rotor, 2017 Far East NDT New Technology & Application Forum (FENDT), 22–24 June 2017, Xi'an, China, <https://doi.org/10.1109/FENDT.2017.8584610>
25. Li X, Sun J, Tao N, et al. An effective method to inspect adhesive quality of wind turbine blades using transmission thermography. *J Nondestruct Eval*. 2018;37(2):19-11. <https://doi.org/10.1007/s10921-018-0473-5>
26. Worzewski T, Krankenhagen R, Doroshnasir M, MathiasRöllig CM, Steinfurth H. Thermographic inspection of a wind turbine rotor blade segment utilizing natural conditions as excitation source, part I: solar excitation for detecting deep structures in GFRP. *Infrared Phys Technol*. 2016;76:756-766. <https://doi.org/10.1016/j.infrared.2016.04.011>

27. Worzewski T, Krankenhagen R, Doroshnasir M. Thermographic inspection of wind turbine rotor blade segment utilizing natural conditions as excitation source, part II: the effect of climatic conditions on thermographic inspections—a long term outdoor experiment. *Infrared Phys Technol.* 2016; 76:767-776. <https://doi.org/10.1016/j.infrared.2016.04.012>
28. A measure white paper for enterprise, drones for wind turbine inspections, measure com, retrieved on April, 22, 2020.
29. Doroshnasir M, Worzewski T, Krankenhagen R, Röllig M. On-site inspection of potential defects in wind turbine rotor blades with thermography. *Wind Energy.* 2016;19:1407-1422. <https://doi.org/10.1002/we.1927>
30. Illingworth J, Kittler J. A survey of the Hough transform. *Comput Vis Graph Image Process.* 1988;44(1):87-116.
31. Ballard DH. Generalizing the Hough transform to detect arbitrary shapes. In: *Readings in computer vision.* Morgan Kaufmann; 1987:714-725.
32. Sezgin M, Sankur B. Survey over image thresholding techniques and quantitative performance evaluation. *J Electr Imaging.* 2004;13(1):146-166.
33. Abu-Ain W, Abdullah SNHS, Bataineh B, Abu-Ain T, Omar K. Skeletonization algorithm for binary images. *Procedia Technol.* 2013;11(0):704-709.
34. U.S. Department of Energy. 2018 Wind Technologies Market Report, retrieved on April 22, 2020.
35. Fingersh L, Hand M, Laxson A. Wind turbine design cost and scaling model. Technical Report NREL/TP-500-40566 December 2006. National Renewable Energy Laboratory.
36. Stiesdal H. unpublished, private communication.
37. MEGAVIND. Megavind LCoE model—guidelines and documentation, 2015.
38. Levy H, Sarnat M. *Capital Investment & Financial Decisions.* Fifth ed. Pearson Education Limited; 1994.

SUPPORTING INFORMATION

Additional supporting information may be found online in the Supporting Information section at the end of this article.

How to cite this article: Chen X, Shihavuddin A, Madsen SH, Thomsen K, Rasmussen S, Branner K. AQUADA: Automated quantification of damages in composite wind turbine blades for LCOE reduction. *Wind Energy.* 2021;24:535–548. <https://doi.org/10.1002/we.2587>

APPENDIX A.: THE DTU SIMPLIFIED COST MODEL

The DTU LCOE model is a simple approach to cost calculation, mainly developed for the assessment of the cost impact of new technologies. It is implemented in an Excel file, see the Supporting Information. The model is based on a simplified cost-scaling method for the turbine cost similar to the approach presented in Fingersh³⁵ and inspired by implementation by Stiesdal.³⁶ The mass of the different components of a turbine is based on scaling equations where the main inputs are the key high-level characteristics of the turbine (i.e., diameter, rated power, and hub height). The mass is converted to a cost estimate using a representative conversion from mass to cost for each component and the total cost of the turbine is the summation of each component's cost. This is the main part of the capital expenditure (CAPEX). In addition to this, overhead, general R&D cost, SG&A, warranty, and profit costs are added. Thus, the total cost represents the sales price of a single turbine. The final element of the CAPEX is the cost of the balance of plant (BOP).

Other elements of the cost model are development costs (DEVEX), abandonment (decommission) costs (ABEX), and the operational expenditure (OPEX) representing the operation and maintenance cost.

The power production (annual energy production [AEP]) is calculated from an assumed turbine capacity factor, which in the model can be assumed to decline annually due to wear.

The cost of energy is levelized, that is, it calculated as the sum of discounted total costs C_d divided by discounted production P_d . The discounting is based on the financial investment decision date (FID), here year 0. The financial modeling is to a large extent based on the MEGAVIND cost model.³⁷

Thus, the levelized cost of energy (LCOE) is calculated as

$$\text{LCOE} = \frac{C_d}{P_d},$$

where

$$C_d = \sum_{t=k}^T \frac{C[t]}{(1+W_n)^t},$$

and

$$P_d = \sum_{t=k}^T \frac{AEP[t]}{(1+W_r)^t}$$

$C[t]$ is the total cost of year t , that is, the sum of CAPEX, DEVEX, OPEX, and ABEX. $AEP[t]$ is the annual energy production for year t . For CAPEX and DEVEX, the actual year can be offset a number of years relative to the FID. W_n and W_r are the nominal weighted average cost of capital (WACC) and the real weighted average cost of capital, respectively.

The relation between these two are

$$W_r = \frac{1+W_n}{1+I} - 1,$$

where I is the inflation rate.

The nominal WACC can either be specified directly as an input or it can be calculated from Levy and Sarnat³⁸:

$$W_n = k_e \left(\frac{S_L}{V_L} \right) + r \left(\frac{B_L}{V_L} \right).$$

S_L is the equity, B_L is the debt, and r is the risk-free interest rate. k_e is based on the expected rate of return on the market portfolio $E(x_m)$ and the firm's systematic risk profile β_i :

$$k_e = r + (E(x_m) - r)\beta_i.$$

The cost model is implemented in an excel file as the DTU LCOE calculator, see the Supporting Information.